ECEN5134 Homework 4

Labib Sharrar

February 21, 2025

1 Problem 1

1.1 (a) Monostatic RCS

First and foremost, we attempt to compute the dimensions of the sphere and the rectangular sheet such that they have the same maximum monostatic RCS value. Before going further, it should be noted that we consider the sides of the rectangle to have the same length. As such the RCS of the rectangular sheet can be written as $\frac{2\pi b^4}{\lambda^2}$, where b is the length of each side. The RCS of the of the sphere, on the other hand can be formulated as πa^2, where a is the radius of the sphere. To find a and b, we equate the RCS equations of the two objects as shown below. In the following equation, we set a to $0.1m$. Since the wavelength used for the simulation is $0.02m$ (at $15GHz$), the radius of the sphere is 5λ.

$$\pi a^2 = \frac{2\pi b^4}{\lambda^2} \tag{1}$$

$$\pi(0.1)^2 = \frac{2\pi b^4}{0.02^2} \tag{2}$$

$$b \approx 0.031 \tag{3}$$

From the above computations, we get $a = 0.1m$ and $b = 0.031$. Next, the sphere and rectangular sheet are designed and simulated on separate FEKO files. To compute the monostatic RCS, σ, a plane wave source is introduced at $\theta = 0°$, making the wave incident to the objects. The plane wave source is also swept from $\theta = 0°$ to $\theta = 180°$, so that we can get bistatic RCS readings. The overall FEKO simulation setup for each object is shown on the next page.

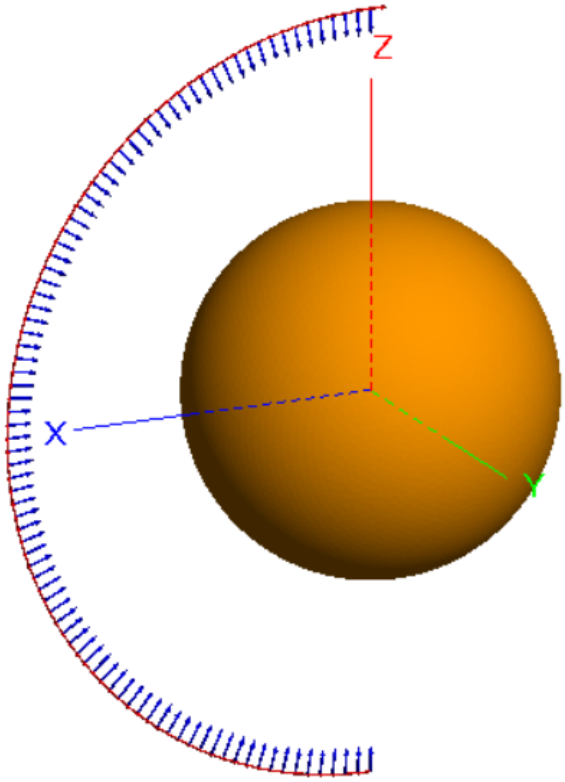

(a) The spherical object with plane waves sent from multiple directions.

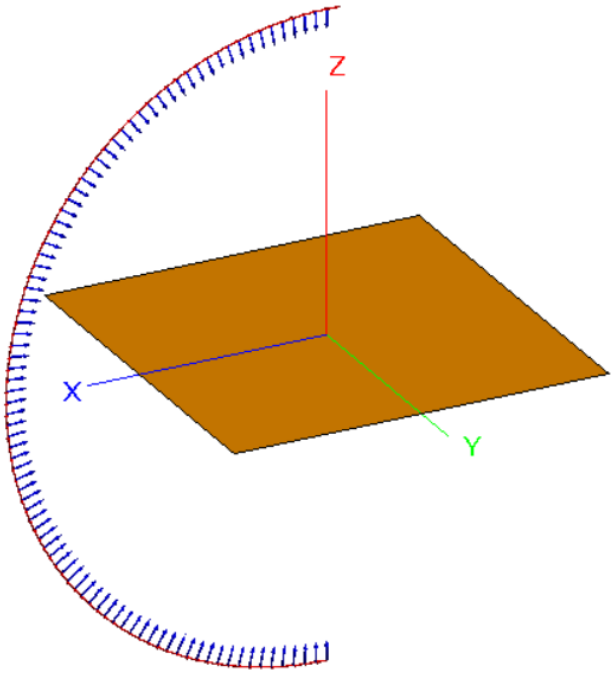

(b) Rectangular object with plane waves sent from multiple directions.

Figure 1: Simulating the sphere and the rectangular sheet in FEKO.

For both the monostatic and bistatic RCS, we can refer to the polar plots shown below.

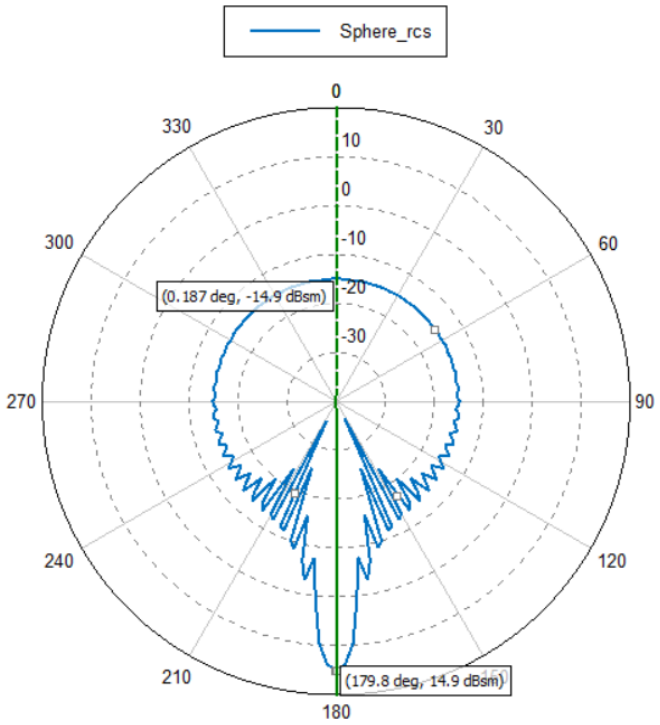

(a) RCS plot of the sphere.

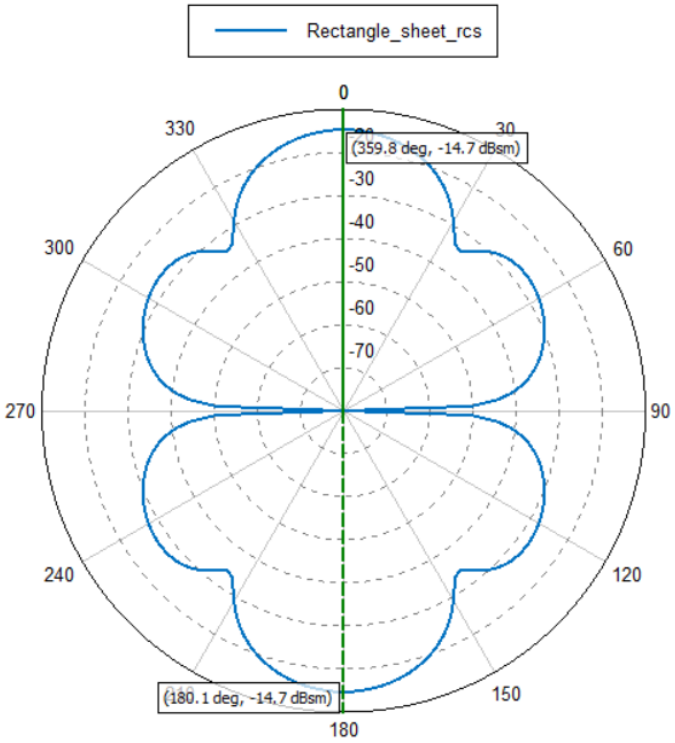

(b) RCS plot of the rectangular sheet.)

Figure 2: Polar plots showing the RCS values of the sphere and rectangular sheet at different θ values.

It should once again be noted that the monostatic incident wave source for each object is placed at $\theta = 0°$. From the polar plots we can clearly see that the monostatic RCS value for the sphere and

rectangle are $-\mathbf{14.9dBsm}$ and $-\mathbf{14.7dBsm}$ respectively. These readings are very close. Thus, we can say that the sphere and the rectangular sheet have the same maximum monostatic RCS value.

1.2 (b) Bistatic RCS

Unlike the monostatic RCS, the bistatic RCS of the two objects are very different. For the sphere, the RCS remains about the same from $\theta = 0°$, but starts to rise as θ approaches 180°. At $\theta = 180°$, the RCS of the sphere spikes up. This happens as a result of the **Mie** scattering effect, also known as the back-scattering enhancement or the creeping wave effect. When an electromagnetic wave interacts with a sphere, some energy wraps around its surface as creeping waves, which re-radiate constructively in the backward direction, enhancing the back-scattered RCS. Additionally, Mie scattering causes resonant interactions, amplifying the signal at $\theta = 180°$, particularly for spheres of moderate to large electrical size. Geometrical diffraction at the rear of the sphere also contributes to this effect. At high frequencies, Bragg scattering further reinforces the peak due to constructive interference between creeping waves and the directly back-scattered wave.

The RCS simulation of the rectangular sheet exhibits a four-lobed scattering pattern, which differs significantly from the smooth, omnidirectional scattering of a sphere. This difference arises from the planar geometry and sharp edges of the rectangular sheet. Unlike a sphere, which scatters energy in all directions with a pronounced backscatter peak at $\theta = 180°$ due to creeping waves, the rectangular sheet produces strong lobes due to specular reflection and edge diffraction. The constructive and destructive interference from these effects results in multiple lobes instead of a single dominant peak. The sheet's sharp edges act as secondary sources of diffraction, causing additional scattering at specific angles, whereas a sphere lacks such discontinuities and follows Mie scattering principles. Furthermore, the RCS pattern of the rectangular sheet is symmetric about $\theta = 90°$.

2 Experiment to Prove Radar Range Equation

As required by the problem, we design an experiment where we have a monostatic setup with a transmitter, receiver and a sphere for scattering. The purpose of this experiment is to ultimately prove the validity of the radar range equation. For the transmitter and receiver, we use a typical dipole antenna that resonates at $15GHz$. We adjust the dipole length to $1.92cm$, and make sure it resonates at $15GHz$ FEKO as shown in the plot below.

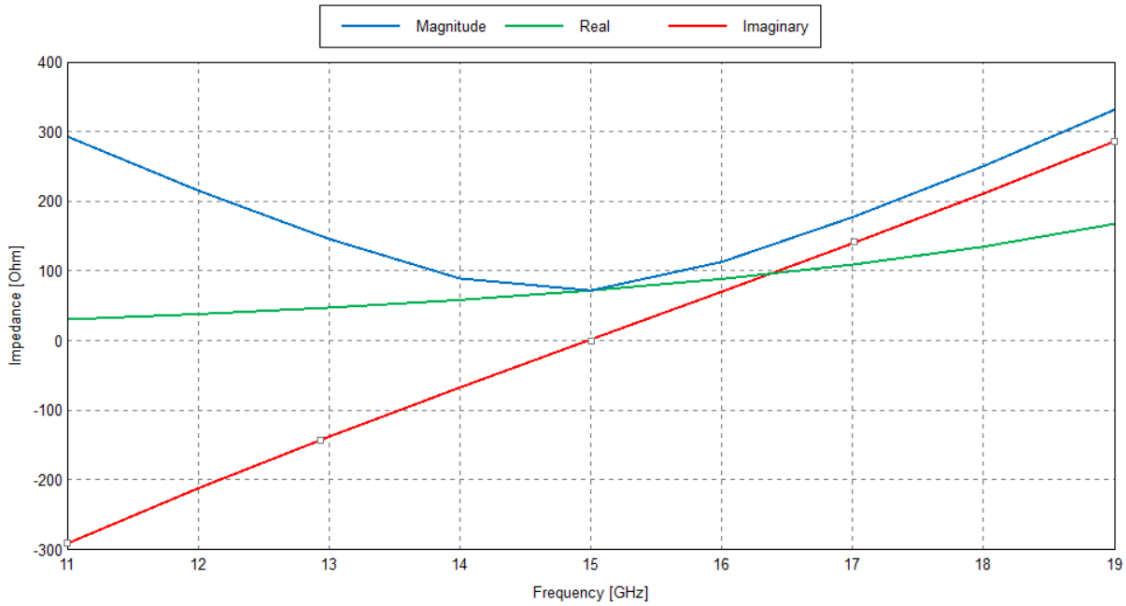

Figure 3: Impedance plot of the dipole across multiple frequencies in FEKO.

Next, we export the far-field pattern of the dipole for later use. As for the scatter object, we construct a sphere of radius $0.02m$ (which is one wavelength long). Compared to the previous experiment,

this sphere has been made considerably small to reduce simulation time. Using a plane wave source, the RCS, σ, of this sphere is found. as illustrated in the images below.

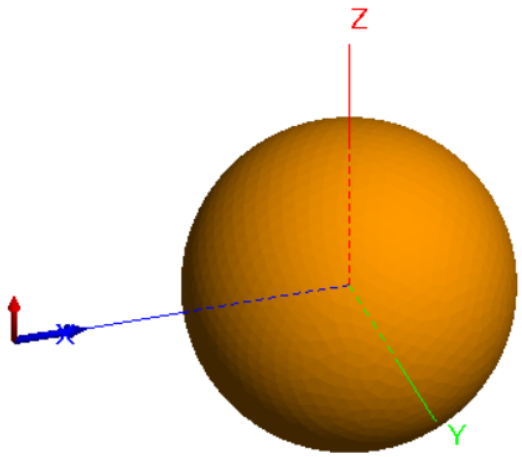

(a) The spherical object with the incident wave at $\theta = 90°$.

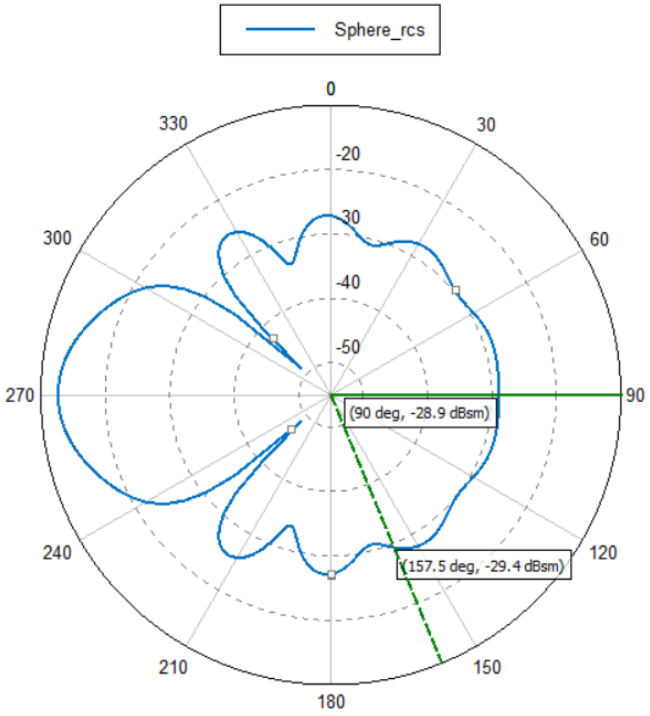

(b) The polar plot to find the RCS (we select the value at $\theta = 90°$.)

Figure 4: Simulating the spherical object.

Since the incident wave is at $\theta = 90°$, we can see that the monostatic σ for this point is $-28.9dBsm$. If we convert this to linear value, we get approximately $\mathbf{1.29 \times 10^{-3} m^2}$. After this, we export the sphere and the dipole antenna we designed to a CADFEKO file. The dipole is placed at coordinates $(x = 0, y = 0, z = 0)$, while the sphere is initially place at $(x = 0.04, y = 0, z = 0)$. The far field of the dipole, based on the formula $\frac{2D^2}{\lambda}$, where D is $0.02m$, is found to be $\mathbf{0.01m}$ away from the dipole. Hence, we ensure that the sphere is placed well into the far field.

So at the moment, we have a transmitter, which is a dipole. The waves from the dipole are scattered off the spherical object. All we need to complete the experimental setup is a receiving antenna. To make the procedures simple, we use the *Receiving Antenna* option in FEKO. From this option, we select *RX far field antenna*. To make this receiver antenna have the same properties as a dipole, we import the far-field patterns of the dipole from the earlier simulations into this receiver antenna as shown in the dialog box below.

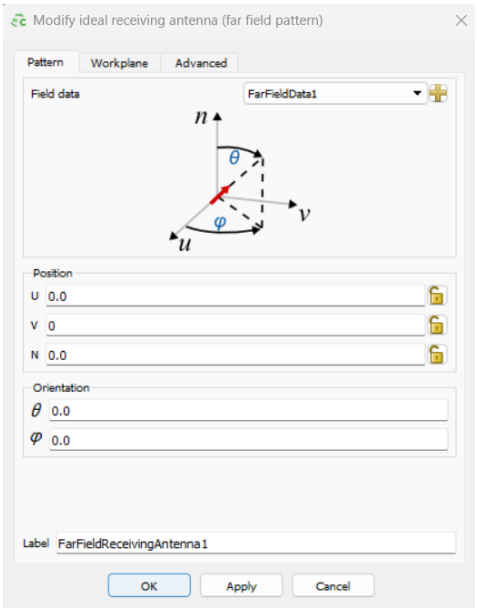

Figure 5: Receiver antenna with the imported dipole far-field patterns.

The receiver antenna, after the modifications (it is basically now a dipole), is place at the origin with the transmitting dipole. Basically, we now have in the setup a transmitting dipole, an identical receiving dipole (made with the *Receiving Antenna* function in FEKO) and the spherical object for scattering the waves. The overall experimental setup is shown in the following image.

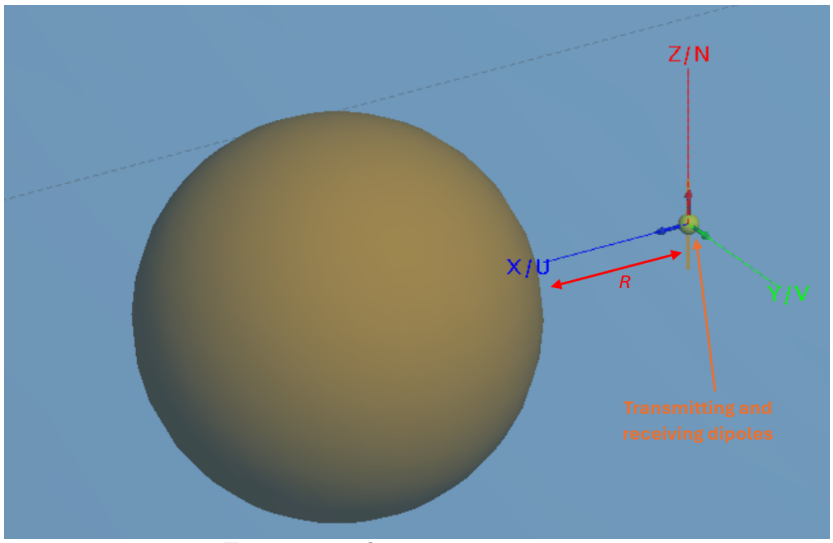

Figure 6: The experiment setup.

We denote the distance between the TX and RX dipoles, and the sphere as R. This FEKO model is simulated for different values of R. At each R value, the transmitted and received power is calculated. In FEKO, we find the transmitted power by measuring the active power at $15GHz$.

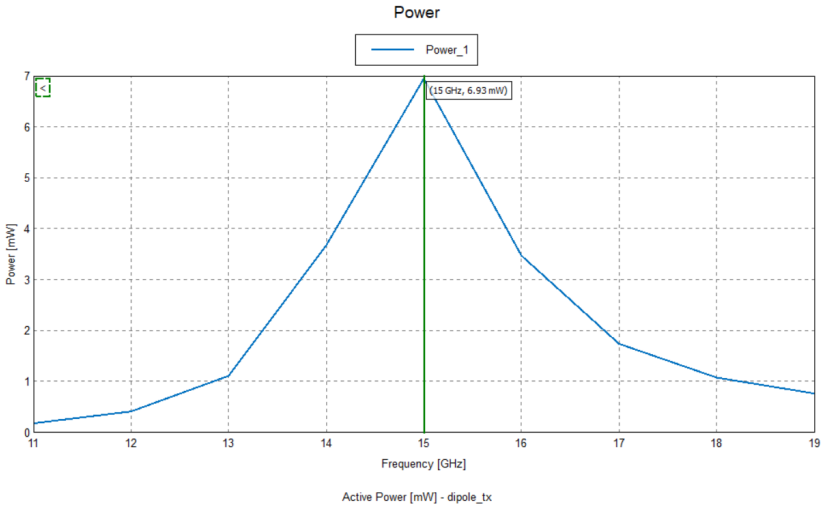

Figure 7: The active or transmitted power.

At $15GHz$, the transmitted power (P_t) by the dipole is found to be $6.93mW$. As the sphere is moved away from the dipoles along the $x - axis$, we measure the received power from the receiver antenna, and record the readings in Table 1. We compare the trend in received power at the receiver antenna, with the theoretical received power (P_r) computed using the radar range equation, which since we have a monostatic setup where the transmitter and receiver are in the same place, can be written as follows.

$$P_r = \frac{\sigma G_{ot} G_{or} \lambda^2}{(4\pi)^2 R^4} \times P_t \tag{4}$$

The notations G_{ot} and G_{or} represent the maximum gains of the transmitter and receiver respectively. Since the two antennas are identical, we consider $G_{ot} = G_{or}$. The value of G_{ot} computed from the dipole simulation is **2.14dBi**, with a linear value of approximately **1.637**.

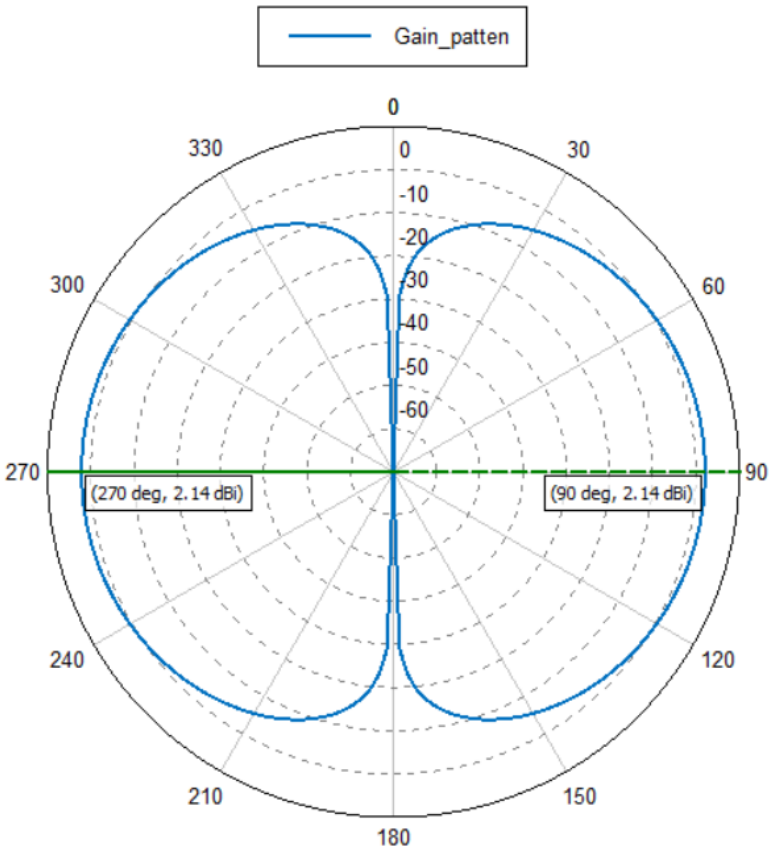

Figure 8: Polar plot showing the maximum dipole gain.

Thus, our constant variables are $G_{ot} = G_{or} = 1.637$, $\sigma = 1.29 \times 10^{-3}$ and $P_t = 6.93mW$. Using these variables we complete the following table. In the table, the column *Theoretical* P_r holds the values computed using the radar range equation in (4).

R (m)	**TX Power** (mW)	**RX Power** (nW)	**Theoretical** P_r (nW)
0.04	6.93	7121	1859
0.05	6.93	2026.7	761
0.06	6.93	773	367
0.08	6.93	184	116
0.1	6.93	64.58	48
0.2	6.93	3.1845	2.97
0.4	6.93	0.187	0.186
0.6	6.93	0.037	0.0367
0.8	6.93	0.012	0.0116
1.0	6.93	0.005	0.0048
1.2	6.93	0.00228	0.00229

Table 1: Received and transmitted power as R increases.

Finally, after recording the data up to $R = 1.2m$ we plot the data from *RX Power* and *Theoretical* P_r to get the following plot. This is done to compare the actual received power, with the theoretical power computed by the radar range equation.

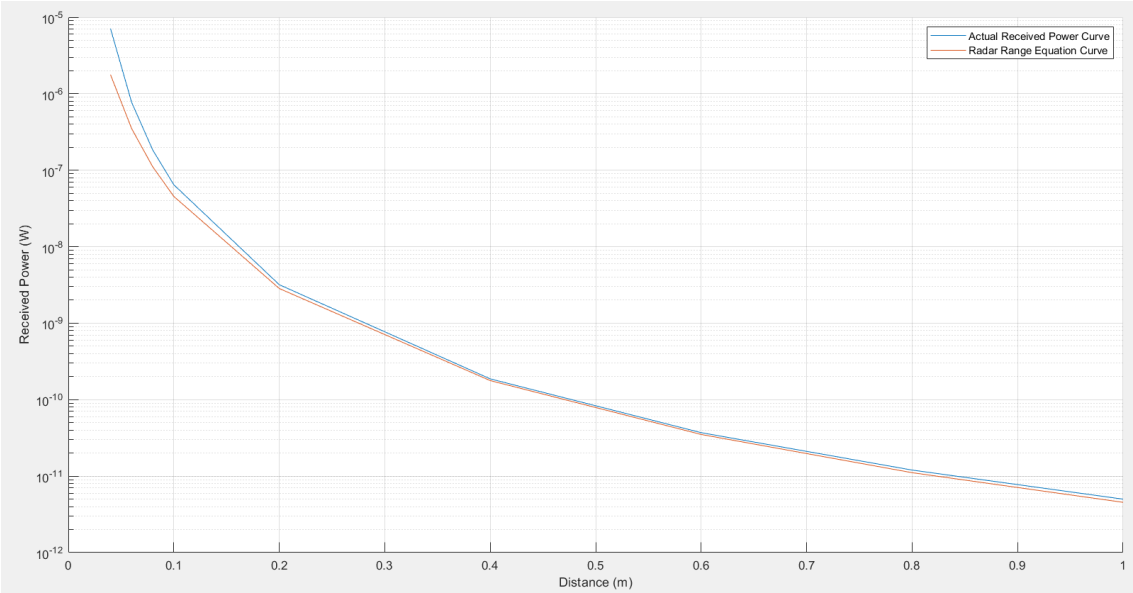

Figure 9: Plot to validate the radar range equation.

From the above plot we can see that the power received by the dipole as the sphere is moved further away follows the same trend and nearly corresponds with the power values computed by the radar range equation. As a result, we can confidently use the results from Table 1 and the above plot to say that the radar range equation is valid.

3 Brightness Formulas (Relative Error)

The formula for computing the spectral brightness radiation by a body, with temperature above $0K$, can be written as follows.

$$B_f = \frac{2hf^3}{c^2} \frac{1}{e^{\frac{hf}{kT}} - 1} \tag{5}$$

In the above equation, the value of the variables h (Planck constant) and k (Boltzman constant) are as follows:

$$h = 6.626 \times 10^{-34} Js$$
$$k = 1.38 \times 10^{-23} JK^{-1}$$

Assuming that the room temperature is $25°C$ we get $T = 300K$. Besides the above equation, there is an approximate formula for computing the spectral brightness as shown in slide 26.

$$B_f = \frac{2kT}{\lambda^2} \tag{6}$$

Equation 5 represents the exact brightness formula, while equation 6 shows the approximate formula which is only valid for $hf << kT$. To compare the two equations, we plot their brightness value for frequencies $1GHz$ to $500GHz$ individually and then plot their relative error.

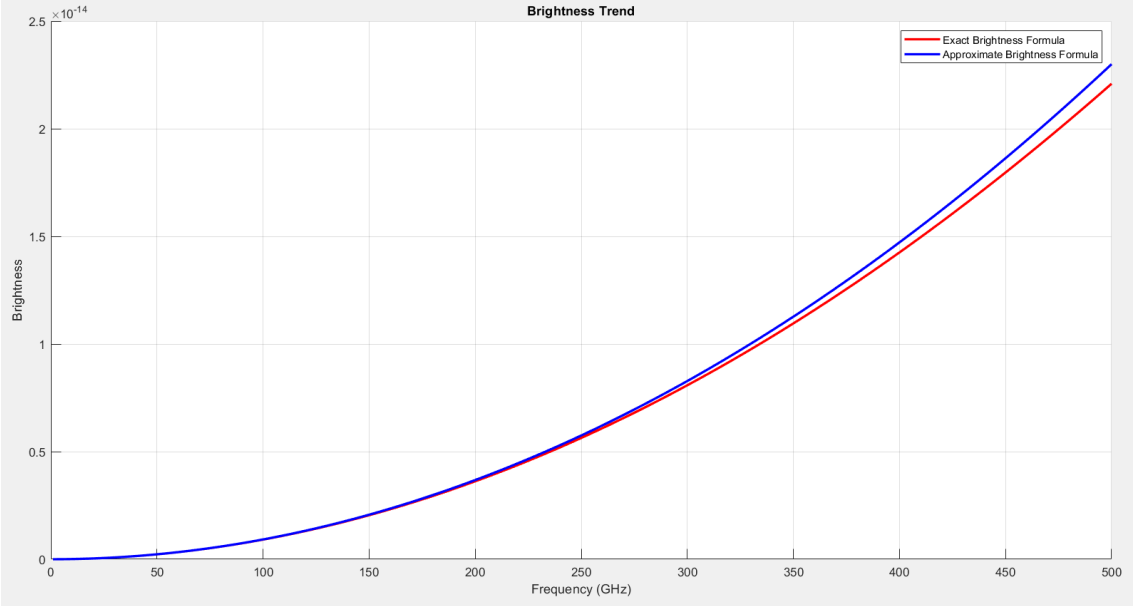

Figure 10: The trend in brightness values for the two equations across different frequencies.

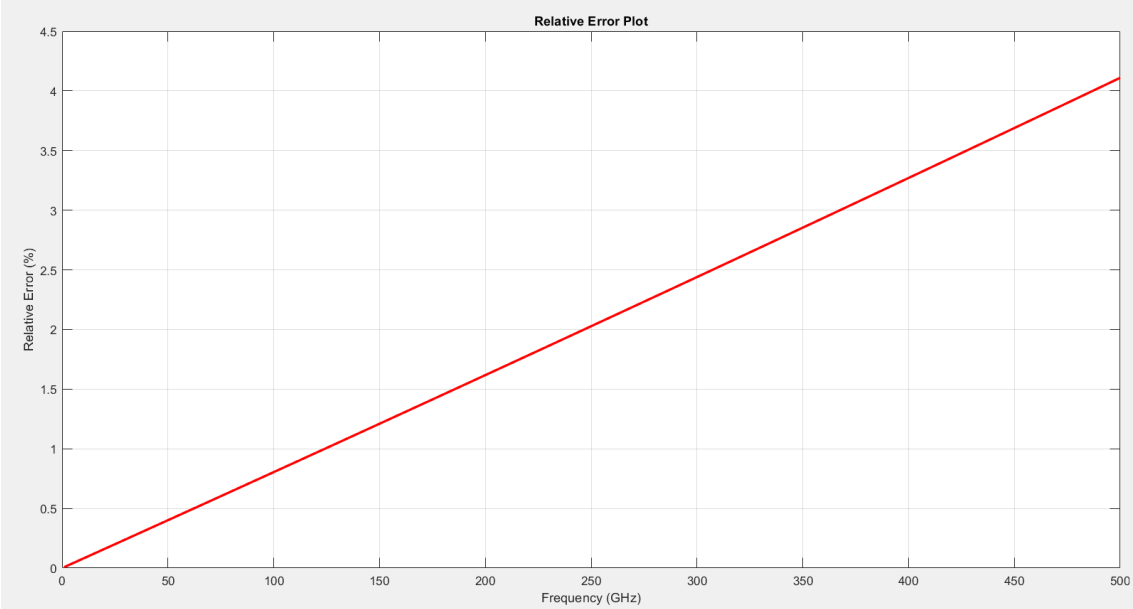

Figure 11: The relative error of the two brightness equations from $100GHz$ to $500GHz$.

From the above plots we see that as the frequency increases, the relative error between the exact and approximate formulas also goes up. This is reasonable since the gap between kT and hf reduces, and the condition $hf << kT$ becomes less valid. Furthermore, in slide 26 we see that the approximate brightness formula is valid to approximately $100GHz$. This matches the results that we have obtained. According to the above plots, the relative error is below 1% for frequencies up to $100GHz$.